Journal of Atmospheric and Solar-Terrestrial Physics 73 (2011) 1201–1213

Contents lists available at ScienceDirect

Journal of Atmospheric and Solar-Terrestrial Physics

journal homepage: www.elsevier.com/locate/jastp

Relating white light and in situ observations of coronal mass ejections: A review

A.P. Rouillard [a,b,*]

[a] College of Science, George Mason University, Fairfax, VA2030, USA
[b] Space Science Division, Naval Research Laboratory, Washington, DC20375-5352, USA

ARTICLE INFO

Article history:
Received 31 March 2010
Received in revised form
3 August 2010
Accepted 26 August 2010
Available online 7 September 2010

Keywords:
Solar wind
White light images
Coronal mass ejections
Magnetohydrodynamics

ABSTRACT

This paper provides a short review of some of the basic concepts related to the observations of coronal mass ejections (CMEs) in white light images and at large distances from the Sun. We review the various ideas which have been put forward to explain the dramatic changes in CME appearance in white light images from the Sun to 1 AU, focusing on results obtained by comparing white light observations of CMEs to the in situ measurements of Interplanetary CMEs (or ICMEs). We start with a list of definitions for the various in situ structures that form an ICME. A few representative examples of the formation of sheath regions and other interaction regions as well as the expansion of magnetic flux ropes are used to illustrate the basic phenomena which induce significant brightness variations during a CME's propagation to 1 AU and beyond. The white light signatures of a number of CMEs observed by the coronagraphs have been successfully simulated numerically by assuming that most of the coronal plasma observed in white light images is located on the surface of a croissant-shaped structure reminiscent of a magnetic flux rope. At large distances from the Sun, white light imagers show that the appearance of CMEs changes dramatically due to the changing position of the CME relative to the Thomson sphere, the expansion of the ejecta and the interaction of the ejecta with the ambient solar wind.

1. Introduction

On 25th October 2006, NASA launched the *Solar-TErrestrial Relations Observatory* (STEREO) on a Delta II 7925-10L rocket from Cape Canaveral Air Force Station in Florida. Each spacecraft used close flybys of the moon to escape into heliocentric orbits near 1 AU, with one spacecraft trailing Earth (STEREO-BEHIND or ST-B) and the other leading Earth (STEREO-AHEAD or ST-A). As viewed from the Sun, the two spacecrafts separate at approximately 45° per year. Along with a comprehensive complement of *in situ* instrumentation, each spacecraft carries a suite of imagers—the *Sun–Earth Connection Coronal and Heliospheric Investigation* (SECCHI) package (Howard et al., 2008). SECCHI consists of an extreme ultraviolet imager (EUVI), two coronagraphs (COR-1 and COR-2), and the *heliospheric imager* (HI). The HI instrument on each STEREO spacecraft comprises two wide-field, visible-light imagers, HI-1 and HI-2. This review discusses the observations of coronal transients made by these imagers. Firstly we describe the relevant physics necessary to understand the STEREO observations. Secondly we describe the STEREO SECCHI and *in situ* instruments used to analyse CME propagation. Thirdly we present a summary of the first STEREO results.

1.1. Coronal mass ejections and streamer activity

Coronal mass ejections (CMEs) are large-scale eruptions of solar material expelled into the solar corona (see for example, the review by Hudson et al., 2006). The basic physical processes that expel these plasma clouds into the heliosphere are still not understood. Solar ejecta, such as CMEs or streamer disconnection events are known to disrupt the more regular spiral distribution of alternating fast and slow solar wind in the interplanetary medium and can trigger strong geomagnetic storms (Burlaga, 1990; Burlaga et al., 1987). Moreover CMEs provide a significant fraction of the average mass flux to the near-ecliptic solar wind, nearly 15% at solar maximum (Webb and Howard, 1994). A CME, strictly speaking, is a phenomenon observed via white light coronal imager. Non-coronagraphic remote-sensing signatures of CME-associated events are numerous (H-α two-ribbon flare/postflare loops, filament disappearance/prominence eruption, Moreoton wave, EIT wave, X-ray eruptive flare, X-ray dimming, EUV dimming, long-decay event, moving type IV bursts, type II bursts). This review discusses CMEs as white light phenomena

* Correspondence address: College of Science, George Mason University, Fairfax, VA2030, USA. Tel.: +1 202 767 2704.
E-mail address: arouilla@gmu.edu

1364-6826/$ - see front matter © 2010 Elsevier Ltd. All rights reserved.
doi:10.1016/j.jastp.2010.08.015

with a brief discussion of a prominence eruption which could have left a strong signal in the spectral band-pass of the white light imagers.

A white light observation results from the integration of sunlight that has been Thomson-scattered by coronal electrons. The scattered light is integrated along the line of sight which imposes certain well-defined observational limits (Vourlidas and Howard, 2006; Howard and Tappin, 2009) which are briefly discussed later in this paper (as well as in Thernisien and Vourlidas, 2010 this issue, and Howard, this issue). Our understanding of the physics of CMEs is based on white light images and has therefore evolved greatly with the changing characteristics of the instruments used to make these observations. The dynamic range, cadence and extent of the field of view of the variety of cameras employed have revealed that the white light signatures of CMEs change dramatically from the Sun to Earth-like distances; a CME event initially observed in coronagraph images will often appear very different at a radial distance of 1 AU.

As we shall see in this review, these changes are not only related to the location and characteristics of the observing cameras, but can also result from the internal evolution of a CME and its interaction with the ambient solar wind. For these reasons we decide to adopt the following terminology. We keep the term CME to refer, in general terms, to coronal brightness variations observed in coronagraph images. However, specific brightness variations observed in images obtained outside the coronagraph field of views, are here referred to as 'density structures'. Density structures may result from a variety of physical processes, associated with the outward propagation of the CME, these processes may be inferred from the results of numerical modelling (Lugaz et al., 2008, 2009) or simultaneous white light and *in situ* measurements (Rouillard et al., 2009b, 2010c).

Three decades of coronagraphic research have revealed the complexity of phenomena which occur during CME eruptions. The source of energy necessary to change the corona and lift CMEs is thought to reside in the photospheric and coronal magnetic fields. Magnetic fields are not observed directly in white light images; however, the high pressure induced by these strong fields can redistribute coronal plasma sufficiently to reveal some of the underlying topology of the magnetic field. White light signatures of CMEs often contain circular features, arches and inter-twined filamentary structures which are reminiscent of helical structures such as magnetic flux ropes. One subset of CMEs can have a well-defined three-part structure consisting of a bright front, dark cavity and core, an observation made during the *Solar Maximum Mission* (SMM) (Illing and Hundhausen, 1986). The bright front has been interpreted as either material swept up by erupting magnetic fields or pre-existing material in the overlying fields (e.g. Sheeley et al., 1999; Riley et al., 2008). The darker region has been interpreted with the presence of organised magnetic fields such as magnetic flux ropes (e.g. Low, 1994; Chen et al., 1997). The bright core can be associated with cool plasma observed in the H-α line of neutral hydrogen but its aspect varies greatly between different CME events. In some events, the bright core appears in coronagraphs after the disappearance of a filament or the eruption of a prominence observed in extreme ultraviolet light and in the H-α line. Bright cores can also appear in white light images without a disappearing filament or an erupting prominence (Robbrecht et al., 2009; Rouillard et al., 2009b). The white light signatures of a number of CMEs observed by STEREO have recently been successfully simulated numerically by assuming that most of the coronal plasma observed in white light images is located on the surface of a croissant-shaped structure, thought to enclose a magnetic flux rope (Thernisien et al., 2009); however, these are indirect inferences only.

CME outflows have been tracked systematically over the last solar cycle by using a variety of techniques. The intensity variation observed in a series of *solar and heliospheric observatory* (SOHO) C2 and C3 coronagraphs difference images, can be extracted along a solar radial corresponding to a constant position angle (PA) and plotted as a function of elongation (*Y*-axis) and time (*X*-axis). Sheeley et al. (1999) revealed, using these 'J-maps', that CME eruptions tend to fall into two (non-distinct) categories; slow ejections ($<400\,\mathrm{km\,s^{-1}}$) rising with a long-lasting ($>6\,\mathrm{h}$) but slow acceleration and faster 'explosive' ejections ($>500\,\mathrm{km\,s^{-1}}$) rising with a high and brief acceleration ($<6\,\mathrm{h}$). The slowly rising mass ejections usually occur without typical eruptive signatures in ultraviolet images (Howard et al., 1985), in stark contrast to the explosive faster ejections which tend to occur at the same time as very energetic events, such as solar flares and prominence eruptions (Andrews and Howard, 2001; Moon et al., 2002; Zhang et al., 2004). A complete solar cycle of these observations has shown that fast ejections are frequent at sunspot maximum when flares and prominence eruptions are more frequent but are rarer at solar minimum (Wang et al., 2006). Many CMEs may not fall in this classification; if the terminal speed is considered alone one finds that all CME speeds taken together do not form two exclusive populations but rather form a continuous smooth distribution (Yurchyshyn et al., 2005).

A third category of streamer ejections is referred to as 'streamer blobs', they appear as slowly rising and poorly defined parcels of coronal brightness variations (Wang et al., 1997, 1998). Streamer blobs are released from the tip of helmet streamers and appear to be entrained by the slow solar wind 'like leaves in wind' (Sheeley et al., 1997). Unlike the well-defined CMEs discussed previously, streamer blobs were not, until the STEREO mission, associated with circular features suggestive of the presence of a magnetic flux rope. The STEREO mission shed new light on the structure of these ejections by offering a set of complementary views; the aspect of streamer blobs can appear very different from two widely separated vantage points; when viewed edge-on, streamer blobs are patches of density variations but simultaneous 'face-on' observations reveal that they are diffuse arches (Sheeley et al., 2009). These images suggest that streamer blobs could be associated with the eruption of magnetic flux ropes, as we shall see, this is suggested by their continual tracking to 1 AU and *in situ* measurements. These images also confirm that white light observations depend critically on the location of the observing camera and the orientation of the mass ejections relative to the observer.

1.2. In situ observations of solar transients

An interplanetary coronal mass ejection (ICME) has been defined as a transient structure observed *in situ* which possesses a combination of physical properties or signatures (rotation of the magnetic field vector, sudden drop in ion temperatures, etc.). Specific combinations of these 'signatures' are required to state that a particular structure observed *in situ* is not quiet solar wind (the simple Parker-type solar wind) but is instead an ICME (Zurbuchen and Richardson, 2006; Jian et al., 2006). Very few ICME events, if any, possess all possible signatures together and usually some three signatures are required to identify an ICME (Jian et al., 2006). The labelling 'ICME', like the labelling CME for white light observations, could therefore incorporate a variety of possible transient structures. Unfortunately there is yet no strict definition of what an ICME represents. Historically, the ICME was the interplanetary signature of a CME, including the whole disturbance: the shock (if existing), the sheath, solar wind pile-up or compression region, 'driver' or ejecta, plus ejecta wake or

CME legs. When the ejecta was associated with a smooth rotation of the magnetic field, a low plasma beta and low temperature it was called a magnetic cloud (MC) (Burlaga et al., 1982; Forsyth et al., 2001). Since that time a fraction of the community has used the term ICME to define the ejecta only, other authors use the term MC to represent any ICME. This is unfortunate, because MCs are a subclass of magnetic flux ropes specific to solar phenomena. In the present paper we propose a set of definitions, specifically designed for the description of simultaneous white light and in situ comparisons:

- An ICME is here defined as the entire solar wind region altered by a solar transient, it includes the shock, sheath, solar wind pile-up, compression regions, driver gas, ejecta wake and/or the legs of magnetic loops. The boundaries of an ICME are defined as the times of exit and entry into calm (Parker-like) background solar wind. The rationale for this definition is that a white light CME is defined broadly as any brightness variation associated with the eruption and propagation of a solar transient (expelled plasma, interaction regions, prominence material, etc.) and does not distinguish between intrinsic CME plasma or plasma that has been accumulated through evolutionary processes, it appears natural that an ICME should also have a broad definition which marks the start and end of disturbed solar wind conditions. We point out to the reader that this definition of an ICME is different to that used by some other authors (e.g. Richardson and Cane, 2010) who use the term ICME to refer to the ejecta only.
- An ejecta is a region of the solar wind which possesses a combination of the following signatures (traditionally at least three, e.g. Jian et al., 2006): rotation of the magnetic field, magnetic field strength enhancement (>10 nT) (Klein and Burlaga, 1982), magnetic field variance decrease (Pudovkin et al., 1979), long time intervals of out-of-ecliptic magnetic fields (Rouillard et al., 2009b), monotonic speed decrease (Klein and Burlaga, 1982; Russell and Shinde, 2003; Démoulin and Dasso, 2009), an extreme density decrease ($<1\,\mathrm{cm}^{-3}$: Richardson et al., 2000), a proton temperature decrease of 50% relative to the ambient wind (Gosling et al., 1973), enhanced alpha to proton ratio ($>8\%$: Hirshberg et al., 1972), elevated oxygen charge states ($O^{7+}/O^{6+}>1$: Henke et al., 2001; Zurbuchen et al., 2003), an unusually high Fe charge states (Bame et al., 1979), the occurrence of He^{+} ($He^{+}/He^{2+}>0.01$: Schwenn et al., 1980), an enhancements of Fe/O, bidirectional strahl electrons (Gosling et al., 1987), bidirectional MeV ions (Palmer et al., 1978).
- A magnetic flux rope (MFR) is a subclass of ejecta, which has the three following properties: drop in field variance, a smooth rotation of the magnetic field vector and an increase of the magnetic field strength near the middle of the rotation. A MFR is not necessarily associated with a drop in temperature or in plasma beta.
- A magnetic cloud (MC) is a subclass of ejecta and of MFRs marked by an extended period with low-beta plasma and low temperature (Burlaga et al., 1981), MCs are often (but not always) preceded by sheaths and interplanetary shocks (Bothmer and Schwenn, 1998).
- A solar wind pile-up is a region of higher solar wind density located around an ejecta.
- A sheath is a subclass of solar wind pile-ups, it is a turbulent and heated region of the solar wind located immediately behind an interplanetary shock, it is usually characterised by high plasma density and higher magnetic field strength and therefore higher total solar wind pressure. The magnetic field is usually drapped around the ejecta and its orientation deviates from the local Parker spiral orientation (Gosling and McComas, 1987).
- Interaction regions are solar wind regions with high total pressure computed from the sum of the magnetic pressure and plasma pressure (Burlaga et al., 2003).

With these definitions MFRs (and therefore MCs) are subclasses of ejecta and are, like sheaths and solar wind pile-ups, the substructures of an ICME. As we shall see, MCs and MFRs are solar wind regions with high magnetic pressure whilst sheaths and solar wind pile-ups often have high plasma pressure, therefore an ICME can be a continuous region of high total pressure sometimes bound by discontinuous drops in pressure marking the presence of forward and reverse shocks. Several ejecta can interact to form a total pressure profile which does not allow by itself to separate the structures that form the different interaction regions; such a region of high total pressure is called a merged interaction region (MIR) (Burlaga et al., 1991, 2003).

By comparing white light and in situ data, we may learn one day that all MFRs have the same origin at the Sun or that MCs result from a different eruptive process than MFRs with higher temperature. A strong association has already been found between MCs and prominence eruptions (Bothmer and Schwenn, 1993). It is by keeping strict definitions for the different measured features that we can reach this goal and perhaps new definitions will be necessary along the way.

The density structures observed in white light images near 1 AU are often associated with density increases inside interaction regions. Three decades of *in situ* measurements have revealed that density variations can result from a variety of processes, three of which are described in Fig. 1 and play a critical role for the white light observations presented later.

- An ejecta can collide with slower plasma, such as slow solar wind, helmet streamers or else slower streamer mass ejections. In this process, shown in Fig. 1a, plasma is swept up and compressed by the fast transient forming an interaction region. Irregularities in the pressure profile are usually removed by compressional waves that radiate away pressure inhomogeneities. However, when the velocity change across the plasma interface exceeds the compressional wave speed, shocks arise and produce discontinuities in pressure and cannot mitigate the steep gradient with small amplitude waves. In this latter case, the interaction region located between the ejecta and the shock is the 'sheath region'.

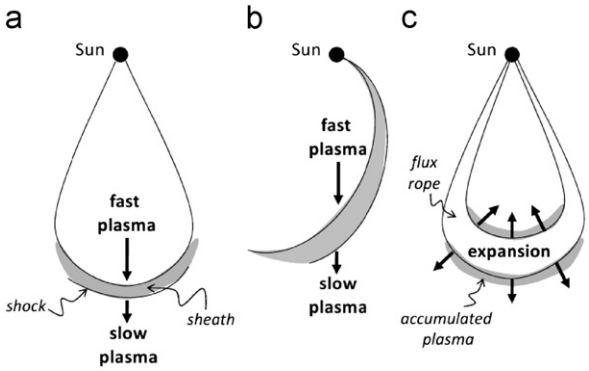

Fig. 1. Three important mechanisms which increase interplanetary plasma density between the Sun and 1 AU. Panel a: Formation of a sheath–shock pair (subclass of interaction regions), panel b: formation of an interaction region ahead of a high speed stream, panel c: plasma accumulation around expanding flux ropes.

- Similar physical processes are observed during the formation of a (corotating/stream) interaction region (CIR/SIR). In this event, shown in Fig. 1b, the fast plasma is a high speed stream which originated in a coronal hole. The corotation of the coronal hole results in the radial alignment of fast and slow solar wind. The kinematic effects associated with fast solar wind catching up slow solar wind induce an increase of plasma density distributed along an Archimedian spiral which is rooted at the Sun (Pizzo, 1982). The dynamic effects, associated with the rise in total pressure inside the SIRs/CIRs, become most apparent beyond 1 AU and can lead to the formation of a forward/reverse shock pair. Unlike the forward shock which propagates into the region of slow solar wind, the reverse shock propagates into the region of fast solar wind where the total pressure is also lower than in the interaction region (Lee, 2000).
- *In situ* observations of MFRs and MCs show that their leading edge typically moves some 30–45 km s^{-1} faster than their rear edge (Burlaga et al., 1981; Klein and Burlaga, 1982; Lepping et al., 2008). These flux ropes are therefore not only expanding in the longitudinal and latitudinal dimensions but they are also expanding along the radial direction. The expansion of the flux rope in the radial direction has been related to the rapid decrease in the total solar wind pressure surrounding the flux rope as it moves away from the Sun (Démoulin and Dasso, 2009; Owens et al., 2006). On average, the front and rear parts of the flux rope separate by a distance of $\sim$0.1 AU during their transit from the Sun to 1 AU. Conservation of mass requires that the rarefaction region induced inside the flux rope is compensated by the accumulation of plasma on the surface of the rope. During their outward propagation, ejecta can over-expand and even form forward-reverse shock pairs (Gosling et al., 1994a,b).

In some complex CME events, the three processes may act together to change the distribution of plasma around the CME. For instance, a CIR may run into an expanding ejecta which is itself compressing the slow solar wind ahead.

The association between CMEs and MCs was made, when a MC was observed by Helios 1 a few days after being observed as a CME by the SOLWIND coronagraphs onboard the U.S. Air Force P78-1 satellite (Burlaga et al., 1982; Sheeley et al., 1985). CME events extending over a large range of PAs in SOHO coronagraph images, termed 'halo mass ejections', are often associated, a few days later, with the passage near Earth of helical magnetic fields. The orientation of eruptive filaments has been related to the orientation of the axis of flux ropes detected *in situ* (Bothmer and Schwenn, 1998). The analysis of the composition of some MCs has revealed high concentrations of Helium and unusual charge-state ratios which have been interpreted as indicative of the presence of filament material (Burlaga et al., 1998). Until the advent of STEREO and SMEI imagers, these associations could only be made by extrapolating the CME path from the Sun to the point of *in situ* measurements, STEREO now enables direct comparison between white light observations and *in situ* measurements.

2. Observations

2.1. SECCHI instruments

The HI detectors are charge-coupled devices (CCDs) with 2048×2048 pixels (N.B.: 1024×1024 pixel synoptic images are routinely downlinked), where each pixel has a size of $13.5 \times 13.5\,\mu m$. HI-1 and HI-2 observe in white light with a band-pass of 630–730 and 400–1000 nm, respectively (Eyles et al., 2009; Harrison et al., 2008; Brown et al., 2009). HI-1 has a 20° square field of view (fov), centered at 14° elongation. The 70° by 70° fov of the outermost HI-2 camera is centered at 53.7° elongation. Note that the elongation of a target is defined as the angle between the observer-Sun vector and the observer-target vector.

To exemplify the geometry of the HI fields of view (fov), Fig. 2a presents a schematic of the ecliptic plane as viewed from solar north on 17 November 2007 showing the relative positions of STEREO-A (ST-A), STEREO-B (ST-B), the Earth (E) and the near-Earth *Advanced Composition Explorer* (ACE) spacecraft. The elongation extents in that plane of the fov of the inner HI-1 and outer HI-2 cameras on STEREO-A (termed HI-1A and HI-2A, respectively) are shown as dot-dashed and continuous black lines, respectively. The extents of the fovs of HI-1A and HI-2A out of the ecliptic plane are shown in Fig. 2c, with the same line styles as in Fig. 1a. Fig. 2b and d presents analogous schematics of ST-B. The elongation, α, of a transient T in the solar wind as observed by either of the STEREO spacecraft is defined as the Sun-Spacecraft-T angle, being zero at Sun center. Fig. 2e and f presents a view of the ecliptic from solar north, like Fig. 2a and b discussed above, illustrating the angular coordinate system used in this paper. The angular separation between the Sun spacecraft line and the direction of propagation of the transient T, β, equates to the longitude separation in an ecliptic-based heliocentric coordinate system (ϕ) when the transient propagates in the ecliptic plane.

Thomson scattering forces geometrical constraints on the part of the solar wind that HI can observe. Solar electromagnetic waves displace coronal electrons in the direction of the oscillating electric field, resulting in electromagnetic dipole radiation. The moving particle radiates most strongly in a direction perpendicular to the electric field (i.e. along the Sun-electron line) so that an observer located at 90° relative to the direction of propagation of the incident electromagnetic wave will observe the least scattered radiation, this radiation will be highly polarized because in this case the observer is situated in the plane of the oscillating electric field. However, at the large distances from the Sun observed by HI, the combination of Thomson scattering with the

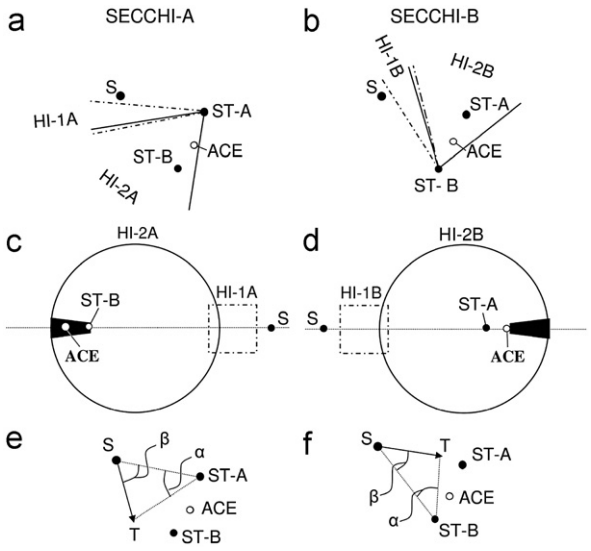

Fig. 2. Panels a and b: Views of the ecliptic plane from above on 17 November 2007 showing the relative positions of STEREO-A (ST-A), STEREO-B (ST-B) and the Earth (E) as well as the extents of the HI-1/2 fovs in the ecliptic plane separately for SECCHI-A and SECCHI-B. Panels c and d: the extents of the fov of HI-1/2A and of HI-1/2B out of the ecliptic plane with the line styles of panels a and b. Fig. 1e and f is the same as Fig. 1a and b but with the angular coordinate system used in this paper and without the fovs shown (Figure taken from Rouillard et al. (2010c)).

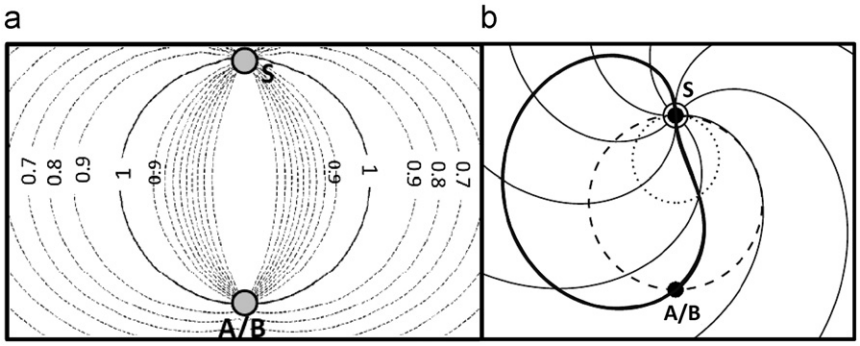

Fig. 3. Panel a: A view of the solar equatorial plane from solar north with the position of the Sun (S) and the ST-A and ST-B spacecraft (A/B) placed at the same location to compare their Thomson spheres. The equicontours of the ratio of the brightness of electrons to their brightness on the Thomson sphere (i.e. maximum value) are plotted along lines-of-sight with elongation angles ranging from 2° to 180° off the east and west limbs of the Sun. Panel b: Also a view of the equatorial plane with the Parker spirals, the Thomson sphere (dashed circle) and the locus of edge-on views of the Parker spiral (continuous black curve).

fall-off with radial distance of solar electromagnetic flux maximises the contribution of scattered light by the electrons that are located closest to the Sun along a particular line of sight. The brightness recorded by a white light imager located at point A/B is therefore maximal for electrons situated near a sphere with as a diameter the Sun-spacecraft segment. This locus traces the points where solar radiation is maximised along different lines-of-sight; the points of closest approach to the Sun. Additionally, coronal electrons are not uniformly distributed along the line of sight of each HI image pixel. Because the sphere represents the points of closest approach to the Sun, solar wind density is also maximised near the sphere, the radial fall-off in electron density will further bias the contribution of electrons located near the sphere. This sphere was termed the Thomson sphere by Vourlidas and Howard (2006) and is also discussed in great detail in Howard and Tappin (2009). Equicontours of brightness values relative to the maximum brightness (i.e. on the Thomson sphere) are plotted in Fig. 3a. These values were computed by combining the effect of the density fall-off with the effect of Thomson scattering (and the associated fall-off in electromagnetic flux). As we can see, electrons located around the Thomson sphere contribute most to the scattered light detected by the observer (value of 1). Interestingly, electrons situated near the Sun-observer line contribute very little to the recorded brightness.

When solar wind transients are entrained and compressed by high speed streams, the compression region tends to be aligned with the plane of the stream interface (the boundary between fast and slow solar wind). In other words, a vector normal to the surface of compression tends to be normal to the local tangent to the spiral formed by the interaction between fast and slow solar wind (so that the plane is roughly aligned with the Parker spiral magnetic field, e.g. Rouillard et al., 2009a). A white light imager integrates light along the line of sight and should integrate more light when it observes a compression region edge-on rather than face-on. Sheeley and Rouillard (2010) derived the equations of the locus of edge-on views of the Parker spiral which is shown in Fig. 3b. The Parker spirals, the Thomson sphere (dashed circle) and a small dotted circle (which we will not discuss here) are also plotted on this view of the solar equator from solar north. The 'locus of enhanced visibility', tracing the locus of edge-on views of the Parker spiral in polar coordinates, is a 'bean-shaped curve' which is asymmetric relative to the Sun-observer line. This asymmetry means that HI-A (looking off the East limb) and HI-B (looking to the West limb) will observe the spiral differently; ST-A will observe the spiral edge-on outside the Thomson sphere whilst ST-B observes the spiral edge-on inside the Thomson sphere. Sheeley and Rouillard (2010) were able to explain a whole range of HI observations related to the compression of streamer blobs by considering the effect of the Thomson sphere together with the effect of the spiral. Tappin and Howard (2009) reached similar conclusions from their analysis of the influence of corotating interaction regions in HI images.

2.2. *In situ measurements*

In addition to the SECCHI imaging suite, each of the STEREO spacecraft also carries a comprehensive suite of *in situ* instrumentation, including the plasma and suprathermal ion composition (PLASTIC; Galvin et al., 2008) and the *in situ* measurements of particles and CME transients (IMPACT; Luhmann et al., 2008) packages. Magnetic field measurements from the magnetometer (MAG; Acuña et al., 2008) and suprathermal electron observations from the solar wind electron analyser (SWEA; Sauvaud et al., 2008), two components of the IMPACT package, are used in the present study together with the solar wind ion moments derived from measurements made by the PLASTIC package. *In situ* measurements of near-Earth solar wind electron and ion as well as suprathermal electrons made by the solar wind electron, proton, alpha monitor investigation (SWEPAM; McComas et al., 1998), solar wind composition measured by the Solar Wind Ion Composition Spectrometer and the Solar Wind Ion Mass Spectrometer SWICS/SWIS (Gloeckler et al., 1998) and measurements of the magnetic field by the magnetic field investigation (MAG: Smith et al., 1998) onboard the advanced composition explorer (ACE) are also used in the present paper. As we shall see, the combination of the STEREO-A and B spacecraft and ACE form an ideal constellation of spacecraft to study solar wind structures near 1 AU. Density and speeds are the two parameters which can be compared between white light and *in situ* measurements directly and are systematically considered in the following discussion of STEREO results.

2.3. *Format of figures*

The combination of STEREO and L1 imaging and *in situ* instruments (more than 18) represents a formidable diversity of datasets. It is therefore easy to lose oneself in this large pool of data, especially in a review paper. This review aims at providing an overview of the STEREO studies which have combined white light and *in situ* measurements. The observations have been classified according to their SECCHI signatures and for each class of events we present a summary of SECCHI and *in situ* measurements. This summary is always presented in the same format and is by no means exhaustive and aims at providing an overview of the observations to the reader. The format of each figure consists

of a single extreme ultraviolet image of the corona near the time of first transient appearance in SECCHI cameras, one running difference image showing the transient in the HIs fov, a set of *in situ* measurements and a J-map establishing the link between the white light and *in situ* measurements.

J-maps are particularly useful in the analysis of HI observations because the time-elongation profile extracted for a given solar transient can be fitted to provide an estimate of its direction of propagation, as well as its velocity (Rouillard et al., 2008; Sheeley et al., 2008a,b; Davies et al., 2009).

Of the available *in situ* measurements we present normalized (at each time step) pitch angle spectrograms of suprathermal electrons at 250 eV from STEREO SWEA and 272 eV from ACE SWEPAM, the strength, azimuth (ϕ) and elevation (θ) angles of the magnetic field, the speed (V), density (n), temperature of solar wind ions. We also present the plasma β parameter calculated as the ratio of the perpendicular plasma (ion and electron) thermal pressure to the magnetic pressure. Due to the lack of continuous alpha and electron particle data for some of the L1 data (ACE and WIND) and the STEREO data, we assume alpha particle number density is 4% of the proton density, alpha particle temperatures of four times the proton temperature and a constant electron temperature of 130 000 K. The latter assumption is consistent with the high thermal conductivity of electrons and the low correlation of electron temperature with other solar wind parameters (e.g. Newbury et al., 1998, and references therein, Issautier et al., 2005). The total perpendicular pressure (P) also presented, is the sum of the magnetic pressure and plasma thermal pressure perpendicular to the magnetic field. The discrepancy between the assumptions and the real values of alpha content and electron temperatures will slightly affect the plasma β and P profiles but provides a more meaningful pressure profile than ion pressure considered alone.

3. STEREO results

3.1. Well-defined CME eruptions with no detected prominence eruption

A CME erupted on 2 June 2008 off the east limb of the Sun as viewed from ST-A whilst appearing at the same time as a Halo mass ejection from ST-B. An HI-1A running difference image and a HI-1/2 A J-map of this event is shown in Fig. 4.[1] Analysis of SECCHI images confirmed that the CME was propagating towards ST-B. The event evolved very slowly and is typical of the streamer-blowout CME class. The CME had a clear three-part structure in COR-2A images, yet none of the STEREO EUVI cameras observed a filament disappearance/prominence eruption prior or during the CME launch (Robbrecht et al., 2009). In fact none of the typical low corona signatures of a CME (flaring, EUV dimming, filament eruption, waves) were observed in the EUVI images. Fig. 4a shows the very quiet state of the corona in EUVI 19.5 nm at the time. The estimated longitude of propagation of the CME is shown by a white circle in this EUVI image. Either, the filament was too small to be observed, was too hot to be detected by EUVI, or there was simply no filament and some CMEs with a bright structures situated at their rear are not associated with a filament eruption (Robbrecht et al., 2009). Wood et al. (2010a) could simulate the time-dependent 3-D changes of coronal brightness around the CME by assuming that the observed plasma is distributed on the surface of a flux rope. The simulation was successful at reproducing many aspects of the leading edge and the rear density structures in all SECCHI cameras. The simulation also provided the tilt of the central axis of the magnetic flux rope relative to the ecliptic plane. They found significant morphological changes of the aspect of this flux rope during its passage though the HI-1A fov. The successes of the white light rendering technique (which does not simulate the formation of interaction regions) in reproducing these changes demonstrates that the appearance of flux ropes can change significantly due to the combined effect of expansion and a variable distance to the Thomson sphere. Wood et al. (2009) used this white light rendering technique to simulate the outward propagation of a more explosive CME eruption (associated with a flare on 26 April 2008) and showed that the different HI instruments can observe very different sections of the same flux rope during its propagation to 1 AU. These studies suggest that a detailed interpretation of HI observations requires some knowledge of the position and orientation of the flux rope relative to the observing camera. The 2 June and 26 April 2008 were neither associated with a disappearing filament nor an erupting prominence. Moreover, Wood et al., 2009 found that the central axis of the 26 April CME flux rope was oriented at an angle of 90° relative to the neutral line of the source region.

Möstl et al. (2009) presented a white light and *in situ* comparison of the 2 June 2008 event which is repeated in part in Fig. 4c–l. The leading density structure and the rear density structure could be tracked from the Sun to STEREO-B and were clearly identified *in situ* as two density increases bounding a magnetic flux rope. This 'hot MFR' was not a MC because the temperature increased rather than decreased towards the center of the rope. We will show another case of 'hot MFR' in Section 3.3. A reconstruction of the magnetic field topology, based on the Grad–Shafranov equilibrium equation (Möstl et al., 2009), showed that the central axis of the helical rope was inclined some 45° relative to the ecliptic which was consistent with the independent white light reconstruction of Wood et al. (2010a). Rouillard et al. (2009b) presented a comprehensive analysis (white light and *in situ* simultaneously) of another solar transient which passed by Venus in May 2007 and also found a good agreement between the orientation of the flux rope determined from *in situ* data by using a force-free field fit and in white light images using rendering techniques.

The flux rope of the 2 June 2008 event was moving some 80 km s^{-1} faster than the solar wind ahead of it and consequently compressed the slow solar wind and drove the formation of a shock. Despite the slowness of this event, the leading density structure developed as plasma was compressed in a 'sheath region'. The leading edge of the rope was moving $\sim$30 km s^{-1} faster than the rear, confirming that the MFR was expanding during its outward propagation. The rear edge of the flux rope was $\sim$60 km s^{-1} slower than the following solar wind, leading to the formation of a small interaction region between the rear of the rope and the faster ambient solar wind. The high total pressure of the expanding rope led to the formation of a reverse shock, this is an example of a forming forward-reverse shock pair in the ecliptic plane. The rear density structure is here interpreted as a weak interaction region formed by the rapid expansion of the rope and its interaction with the ambient solar wind. We note that this rear density structure contrasts with the classic interpretation of the bright core that is often observed by coronagraphs towards the back-end of CME flux ropes (i.e. at the rear of cavities). The white light simulations of Wood et al. (2010a) suggested that the flux rope was expanding along the radial direction but not in a self-similar manner, the interactions between the MFR and the ambient solar wind perhaps prevented the MFR from expanding

[1] Movie versions of STEREO and SOHO images shown in Figs. 4–7 are available on the NRL SECCHI website at http://secchi.nrl.navy.mil/index.php?p=js_secchi and on the UK STEREO website at http://www.ukssdc.ac.uk/solar/stereo/movies/MOVIES/

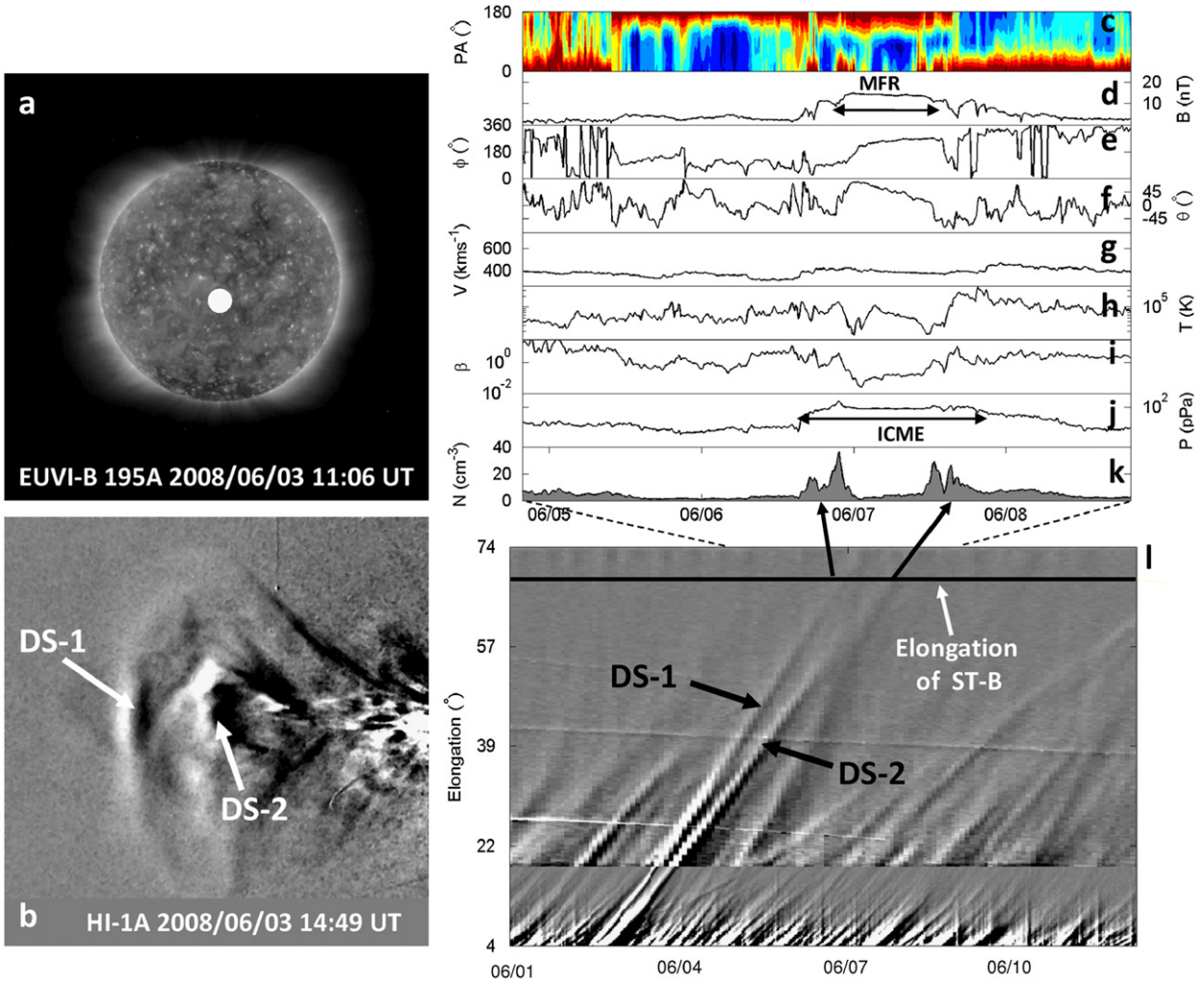

Fig. 4. A summary of observations described in detail in Section 3.1 for the 2 June 2008 CME. (a) is an EUVI image at 19.5 nm from ST-B. The white light observations are from HI1-A (b) and HI-1/2A (J-map in (l)). The density structures (DS) observed in HI and discussed in the text are indicated. The *in situ* measurements were obtained by ST-B. The white circle on the EUVI image is the estimated longitude of the source region of the CME.

self-similarly. Unfortunately, the authors do not state the exact type of expansion found but previous studies have found that ICMEs elongate kinematically in angular extent during their outward propagation (e.g. Owens et al., 2006; see review paper by Crooker and Horbury, 2006).

Savani et al. (2010) used HI observations and numerical simulations to study an extreme case of interaction between a flux rope and its surrounding solar wind. The flux rope, observed edge-on, started as a quasi-circular structure in COR-2B and changed into a bean-shaped structure following its interaction with the ambient solar wind. No *in situ* measurements were available for this event; however, it is likely that total pressure was greatly enhanced inside and around this flux rope. The following example presents a direct association between well-defined interaction regions observed *in situ* and large-scale density structures observed in white light images.

Fig. 5 presents, in the same format as Fig. 4, observations of the outward propagation of density structures associated with a MC detected near Earth on 19–20 November 2007. Like the 2 June event, two density structures can be tracked from the Sun to 1 AU for this event. The passage of the rear density structure is immediately followed by the arrival of high speed streams. Rouillard et al. (2010c) identified the leading density structure as a sheath region and the rear density structure as an interaction region formed by high speed streams compressing the rear of the MC. The trailing density structure is already a large structure (width greater than 5° elongation) when it is first evident in the HI-2B difference images ($\alpha \sim 20^{\circ}$) suggesting that compression may have already started at a heliocentric radial distance of 0.3–0.5 AU. Comparison of the HI-A and HI-B observations showed that HI-B observed the rear density structure more clearly than HI-A. This was partly associated with the fact that HI-B integrated more sunlight along the plane of CIR-CME interaction (viewing the CIR spiral edge-on) than HI-A which integrated sunlight across this plane (see Section 2.1). The reader is referred to the paper by Sheeley and Rouillard (2010) which discusses this effect in more detail.

The combination of the sheath region, the MC and the interaction region between the MC and the high speed stream forms a continuous region of high total pressure or MIR (Burlaga et al., 1991, 2003). The formation of MIRs is more common near and beyond 5 AU where the entrainment of transients by high speed streams is common (Burlaga et al., 2003). This analysis showed that the onset of MIR formation can occur as close as 0.3 AU from the Sun. Moreover, this analysis exemplifies the inadequacy of the term CME in describing density structures in the HI-2 field of view. Density structures can contain as much if not more plasma that is kinematically and dynamically gathered by the interaction of the flux rope with ambient solar wind than intrinsic plasma released with the 'coronal mass ejection'.

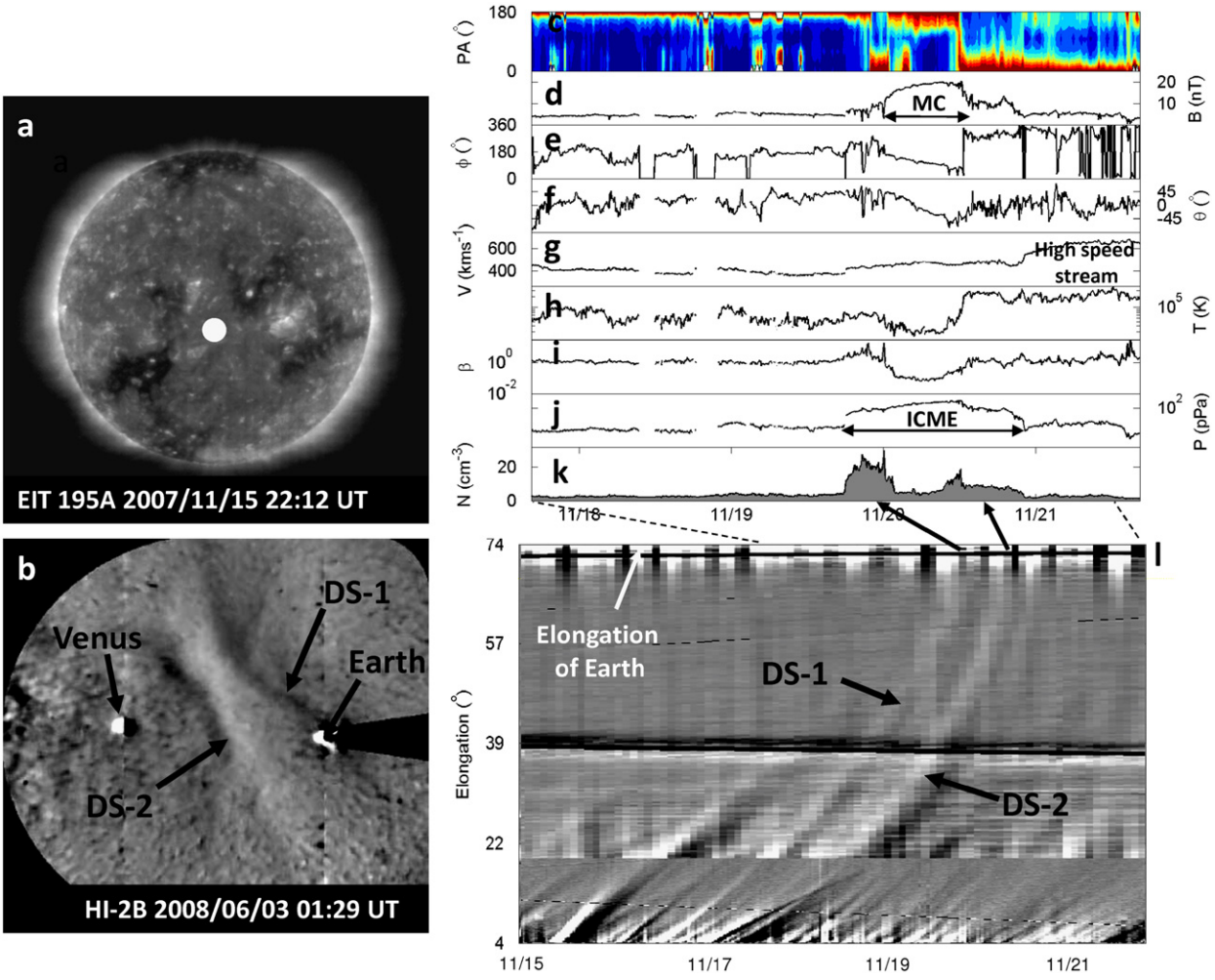

Fig. 5. A summary of observations described in detail in Section 3.1 for the 15 November 2007 CME. (a) is an EIT image at 19.5 nm from ST-A. The white light observations are from HI-2B (b) and HI-1/2B (J-map in (l)). The *in situ* measurements were obtained by ACE.

It appears impossible to distinguish, from white light images alone, which plasma has been ejected from the Sun in the CME event and which plasma has been accumulated through evolutionary processes (kinematic gathering, compression, etc.). Lugaz et al. (2008) showed, through numerical simulations, that interaction regions can occur between two out-flowing CMEs or when high speed streams catch up slow CMEs (such as the event shown in Fig. 5), and confirmed that the increase in density associated with these interaction regions is a prime source of coronal brightness variations in HI images.

3.2. *Poorly defined eruptions with no detected filament activity*

Some streamer events are associated with very small changes in coronal brightness and can remain largely undetected in the COR-1 and COR-2 fov. These ejections can become apparent higher up in the solar atmosphere due to their interaction with the ambient solar wind. For instance, the plasma density along the sunward edge of these structures can be enhanced when they are caught up and entrained by high speed streams (in the HI-1 fov but mostly in HI-2 fov). Streamer blobs ejected from an inclined streamer (i.e. face-on blobs) can fall in this category, they remain very faint or unresolved in COR-2 running difference images but can evolve into large-scale density structures near 1 AU (Sheeley and Rouillard, 2010). As described in Section 1.1, STEREO has revealed that many of these streamer blobs are actually arch-like structures reminiscent of magnetic loops (Sheeley et al., 2009) and could be considered very small CMEs. The term blob is probably not adequate anymore and we should perhaps call these structures ‘streamer arches’.

Fig. 6 presents a case of poorly defined eruption, the aspect of this ejection evolved from an arch-like feature in the COR-2B fov into a large-scale density structure in the HI-2B fov. In contrast to the previous examples of larger ejections, HI-2 only observed a single large-scale density structure with this event. According to the track fitting procedure that we use routinely only one of the two traces seen in the J-map of Fig. 6 is associated with the streamer arch tracked to the in situ instruments located near 1 AU, the second track was associated with another transient propagating along a different longitude. The arrow points to the track which impacted ACE.

The ACE spacecraft detected the *in situ* signature of this density structure; a region of enhanced plasma density associated with an interaction region located between a high speed stream and an average size MC with a radial dimension of 0.2 AU (Rouillard et al., 2010a,b). No density increase was observed ahead of the MC because it was propagating (was convected) at the ambient solar wind speed. The magnetic field strength is smaller than the average magnetic field strength of MCs (>10 nT). More examples of these weak streamer ejections have been published and confirm that they are either undetected in COR-2 or else appear

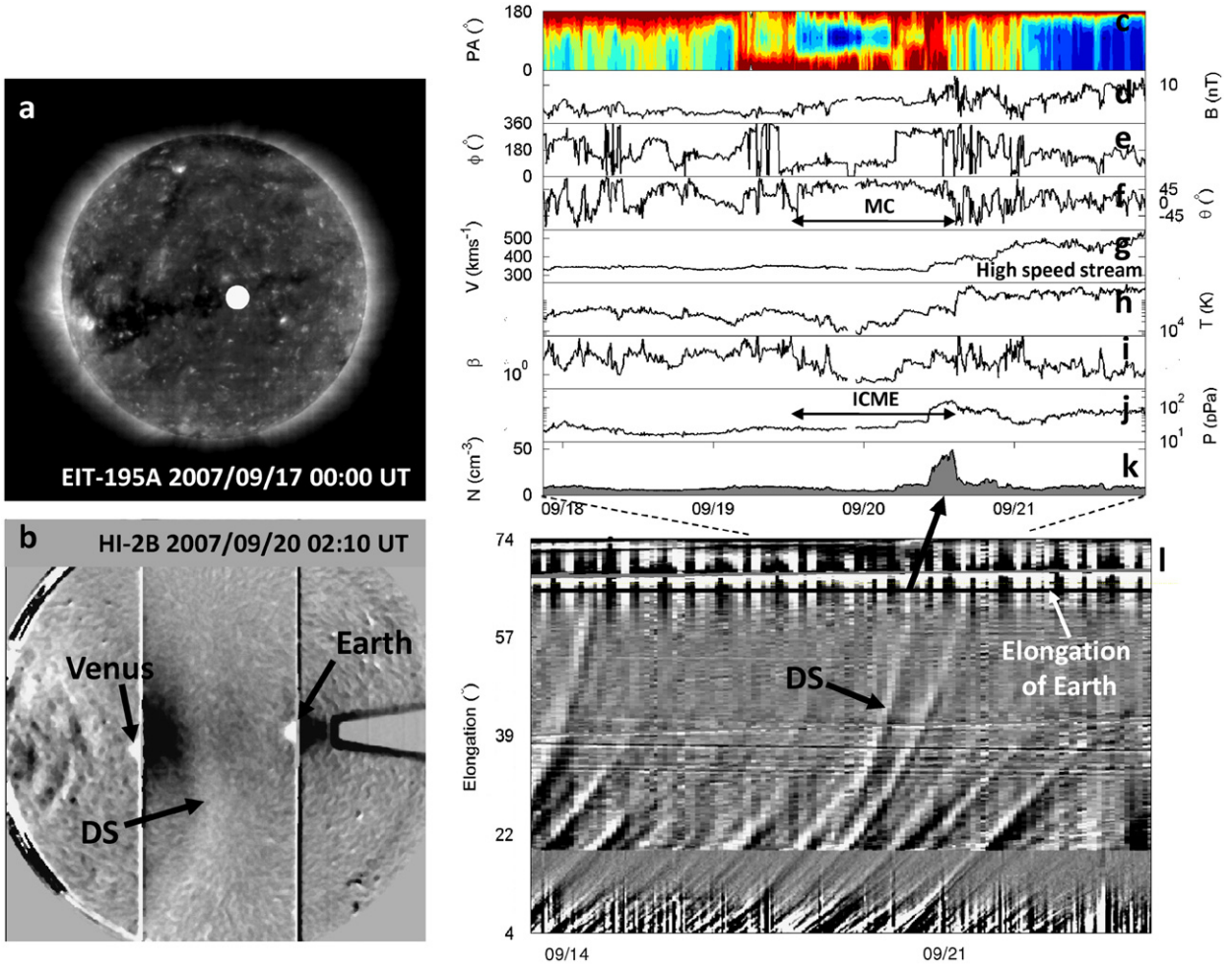

Fig. 6. A summary of observations described in detail in Section 3.2 for the 17 September 2007 transient. (a) is an EIT image at 19.5 nm from SOHO. The white light observations are from HI-2B (b) and HI-1/2B (J-map in (l)). The *in situ* measurements were obtained by ACE/WIND.

as small loops, but that they can be swept up by high speed streams and revealed higher up in the corona. It has been found that the magnetic field strength is typically weak inside these events (<10 nT) (Kilpua et al., 2009). This confirms that HI-2 provides a complementary view of streamer outflows to the standard coronagraphs. Moreover, these ejections can be used as 'tracers' to track the progression of CIRs in white light images (Rouillard et al., 2008; Sheeley et al., 2008a,b; Howard and Tappin, 2009; Wood et al., 2010b). *In situ* observations of the slow solar wind reveal the presence of many small-scale transients associated with counter-streaming electrons (like the transient passage shown in Fig. 6c) which could be additional *in situ* signatures of these poorly defined ejections (Kilpua et al., 2009). According to our set of definitions (Section 1.2), ACE enters the ICME event shown in Fig. 6 at the time of entrance of the MC and exits the ICME when it enters the region of high speed stream. Streamer arches that are swept up by high speed streams are therefore characterised by a highly asymmetric pressure profile, the total pressure remains relatively flat throughout the event and peaks inside the interaction region located at the back-end of the event.

3.3. Large eruptions with detected filament activity

None of the mass ejections discussed so far in this review paper were associated with the detected eruption of a prominence (or disappearance of a filament). Yet the eruption of a prominence has been associated in previous studies with strong signatures in coronagraph images because they carry dense plasma (Illing and Hundhausen, 1986). Solar prominences consist of relatively cool, dense plasma that is suspended in the solar corona at heights up to 100 Mm above the chromosphere. The H-α 656.3 nm line of neutral hydrogen is the principal prominence spectral line observed in the SECCHI white light instruments (spectral band-passes are for COR1: 543–786 nm; COR-2: 650–750 nm; HI-1: 630–730 nm; HI-2: 400–1000 nm). The magnetic structure of prominences is still not understood, with many observations and theoretical models differing on the exact nature of the magnetic field (see the review by Mackay et al., 2010).

In December 2008, a CME entered the COR-1A and COR-1B fov soon after the ejection of a prominence detected in EUVI-A and EUV-B images (in the He II spectral line of 30.4 nm). The ejection could be followed from the Sun to Earth in all the SECCHI-A and SECCHI-B white light instruments (Davis et al., 2009). Fig. 7 shows, again in the same format, the SECCHI and *in situ* measurements of this event. The HI-1B image reveals the complexity of the internal structure of this solar event; many disjointed density structures are observed and do not form a clear pattern like the 17 November 2007 and 02 June 2008 events which were associated with two large-scale density structures. Unlike the November 2007 event, the density structures are already bright structures inside the HI-1 fov. Davis et al. (2009) and Liu et al. (2010) tracked three-density structures to 1AU and could identify their *in situ* signatures at L1. The two leading

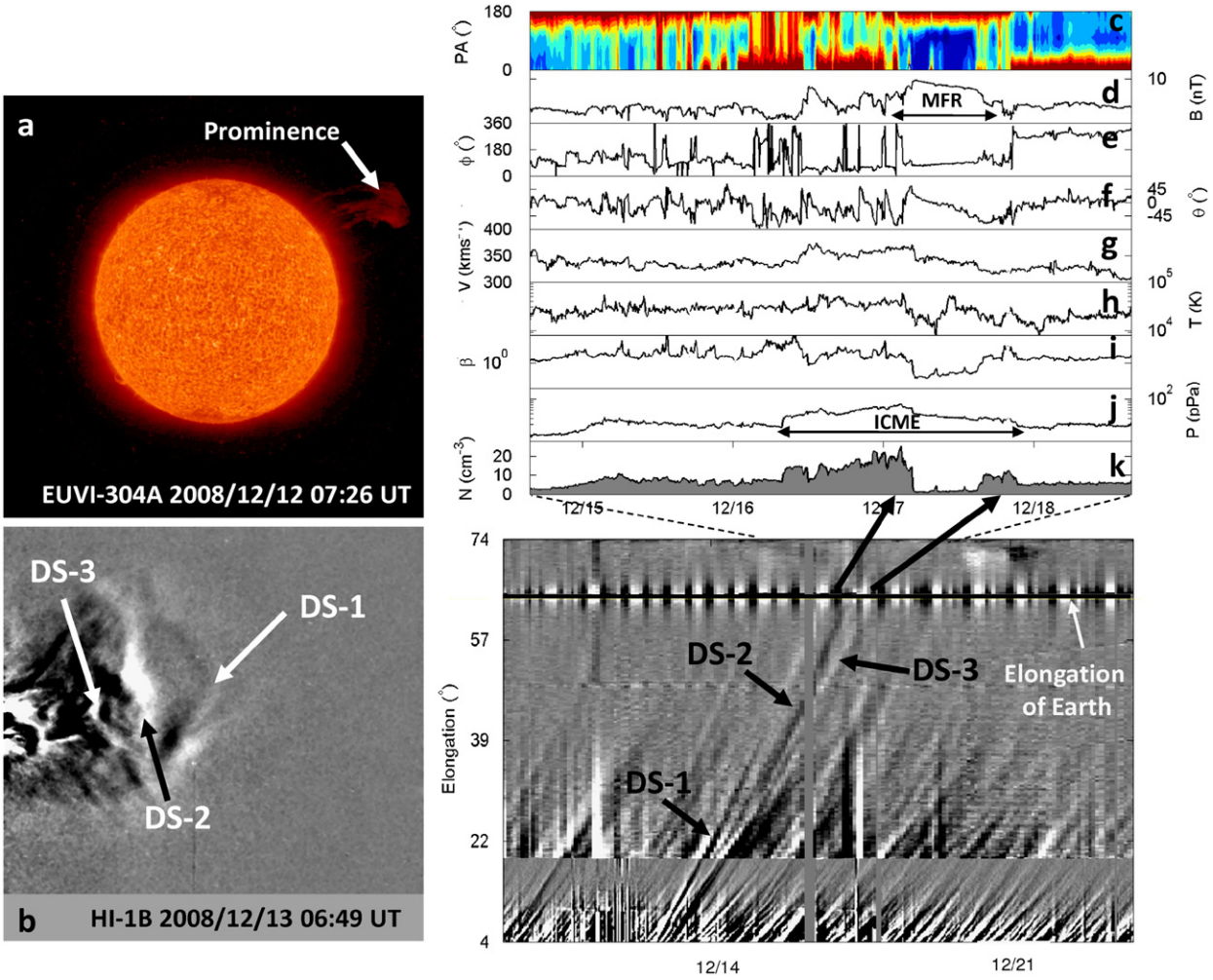

Fig. 7. A summary of observations described in detail in Section 3.3 for the 12 December 2007 CME. (a) is an EUVI image at 30.4 nm from ST-B. The white light observations are from HI-1B (b) and HI-1/2A (J-map in (l)). The *in situ* measurements were obtained by ACE/WIND.

density structures preceded the arrival of a MFR, the third density structure marked the end of the MFR passage. The solar storm was propagating with the same speed as the surrounding solar wind and it is unlikely that the origin of the density structures surrounding the MFR resides in interaction regions only. The MFR was expanding at 1 AU and this expansion probably contributed to the intensification of the density structures surrounding the MFR. It is likely that the complexity of the density structures at the rear of the event were related to the erupting prominence however more detailed analysis of this event is required to verify that.

3.4. Discussion and conclusion

The observational heritage of SMM, SOLWIND, and SOHO has taught us that fast CMEs can interact significantly with the ambient corona already inside the coronagraph fov. The necessity of a multiperspective and multipoint mission to disentangle the various processes at play during a CME's propagation to 1 AU became apparent from the International Solar Terrestrial Physics (ISTP) programs which focused, during the early years of SOHO, on the Sun–Earth connection. The Earth-directed CMEs which emerged on the rising phase of cycle 23 (such as the 10 January and 12 May 1997 events) were particularly suitable for studying the Sun–Earth connection, eruptive filaments and the interaction between CMEs and the background solar wind (Burlaga et al., 1987; Plunkett et al., 1997; Webb et al., 2000; Arge et al., 2004). Now, STEREO allows us to study these interactions from two vantage points and in 3-D. Techniques which can determine the 3-D topology of the magnetic field measured *in situ*, such as force-free field fits and Grad–Shafranov reconstructions of flux ropes, provide estimates of the local topology and orientation of MFRs and MCs. So far, the results of these techniques in determining the large-scale geometry of flux ropes have only been compared to white light simulations for a handful number of cases. More comparisons between white light rendering techniques (Thernisien et al., 2009; Wood et al., 2009) and flux rope reconstructions (Rouillard et al., 2009b; Möstl et al., 2009) are necessary to assess the validity of these models. These types of studies may lead to a better forecasting of southward pointing magnetic fields which is critical for predicting geomagnetic activity.

The studies reviewed in the previous paragraphs have shown that the major changes in the appearance of solar storms observed in white light imagers are a convolution of:

- the changing position of the density structures relative to the Thomson sphere,
- internal evolution of the storm (e.g. expansion of MFRs and MCs),

- the interaction of the storm with the 'background' solar wind (the fast and slow solar wind),
- the release of plasma via the eruption of prominence material (observed through the scattering of the ejected electrons and through the emission of H_α neutral hydrogen).

SECCHI observations show that the appearance of CMEs in coronagraphs observations is consistent with that expected of plasma distributed on the surface of a croissant-shaped flux rope (Thernisien et al., 2009; Wood et al., 2010a), but that out in the solar wind, the appearance of CMEs depends on other effects: its position relative to the Thomson sphere, its internal evolution and interaction with the background solar wind. White light observations detect the influence of the invisible magnetic field (like a 'moving ghost') on the surrounding solar wind. In particular, the internal pressure of the flux rope and its interaction with the solar wind are fundamental processes that will change some of the key solar wind parameters that control magnetospheric activity such as the magnitude of southward pointing magnetic fields, density, and dynamic pressure. The largest geomagnetic storm of 2007 was generated by a MC with intense southward IMF which was generated by the compressive effects of high speed streams running into the back-end of the MC, an interaction clearly detected in SECCHI images (Rouillard et al., 2010c). SECCHI has shown that fast solar wind can compress flux ropes already at a radial distance of 0.3 AU, in agreement with Helios in situ measurements (Gulisano et al., 2010). It also showed that the expansion of flux ropes increases plasma density around the surface of the rope.

These interactions should lead to significant alterations of the flux rope topology. In particular, reconnection between flux ropes and the overtaken magnetic field may occur frequently in the solar wind (Dasso et al., 2007). Numerical studies have shown that the interaction between transients and between transients and the background solar wind could also lead to very large reconnection *X*-lines forming in the lower corona and thereby leading to the coalescence of a flux rope with another flux rope (e.g. Xiong et al., 2007, 2009) or between a flux rope and the background magnetic field well inside 1 AU (e.g. Schmidt and Cargill, 2003; Manchester et al., 2004). Could such large-scale merging events leave white light signatures?

STEREO is still a young mission and exciting new results are waiting to be found in the unique datasets which are created every day.

Acknowledgements

The author wishes to thank Jackie Davies, Neil Sheeley, Benoit Lavraud, Yi-Ming Wang and Mike Lockwood for their continuous scientific and technical support as well as all the scientist and engineers which have contributed to the STEREO mission. The author also thanks the two referees for their detailed and very constructive reports which have greatly improved this review. The STEREO/SECCHI data are produced by a consortium of RAL (UK), NRL (USA), LMSAL (USA), GSFC (USA), MPS (Germany), CSL (Belgium), IOTA (France) and IAS (France). The ACE data were obtained from the ACE science center. This work was supported by NASA.

References

Acuña, M.H., Curtis, D., Scheifele, J.L., Russell, C.T., Schroeder, P., Szabo, A., Luhmann, J.G., 2008. The STEREO/IMPACT magnetic field experiment. Space Science Reviews 136 (1–4), 203–226.

Andrews, M.D., Howard, R.A., 2001. A two-type classification of lasco coronal mass ejection. Space Science Reviews 95 (1/2), 147–163.

Arge, C.N., Luhmann, J.G., Odstrcil, D., Schrijver, C.J., Li, Y., 2004. Stream structure and coronal sources of the solar wind during the May 12th, 1997 CME. Journal of Atmospheric and Solar-Terrestrial Physics 66 (15–16), 1295–1309.

Bame, S.J., Asbridge, J.R., Feldman, W.C., Fenimore, E.E., Gosling, J.T., 1979. Solar wind heavy ions from flare-heated coronal plasma. Solar Physics 62, 179–201.

Bothmer, V., Schwenn, R., 1993. Eruptive prominences as sources of magnetic clouds in the solar wind. Space Science Reviews 70, 215–220.

Bothmer, V., Schwenn, R., 1998. The structure and origin of magnetic clouds in the solar wind. Annales Geophysicae 16 (1), 1–24.

Brown, D.S., Bewsher, D., Eyles, C.J., 2009. Calibrating the pointing and optical parameters of the STEREO heliospheric imagers. Solar Physics 254 (1), 185–225.

Burlaga, L., Sittler, E., Mariani, F., Schwenn, R., 1981. Magnetic loop behind an interplanetary shock-Voyager, Helios, and IMP 8 observations. Journal of Geophysical Research 86 (August 1), 6673–6684.

Burlaga, L.F., Klein, L., Sheeley Jr., N.R., Michels, D.J., Howard, R.A., Koomen, M.J., Schwenn, R., Rosenbauer, H., 1982. A magnetic cloud and a coronal mass ejection. Geophysical Research Letters 9, 1317–1320.

Burlaga, L.F., Behannon, K.W., Klein, L.W., 1987. Compound streams, magnetic clouds, and major geomagnetic storms. Journal of Geophysical Research 92, 5725–5734.

Burlaga, L.F., 1990. Coalescence of recurrent streams of different sizes and amplitudes. Journal of Geophysical Research 95, 4247–4255.

Burlaga, L.F., Hewish, A., Behannon, K.W., 1991. Structure and evolution of compound streams at not greater than 1 AU. Journal of Geophysical Research 96 (December 1), 21213–21225.

Burlaga, L.F., Fitzenreiter, R., Lepping, R., Ogilvie, K., Szabo, A., et al., 1998. A magnetic cloud containing prominence material: January 1997. Journal of Geophysical Research 10, 277–285.

Burlaga, L.F., Berdichevsky, D., Gopalswamy, N., Lepping, R., Zurbuchen, T., 2003. Merged interaction regions at 1 AU. Journal of Geophysical Research 108 (A12. doi:10.1029/2003JA010088.

Chen, J., Howard, R.A., Brueckner, G.E., Santoro, R., Krall, J., et al., 1997. Evidence of an erupting magnetic flux rope: LASCO coronal mass ejection of 1997 April 13. Astrophysical Journal Letters 490, L191.

Cooker, N.U., Horbury, T.S., 2006. Solar imprint on ICMEs, their magnetic connectivity, and heliospheric evolution. Space Science Reviews 123 (1–3), 93–109.

Davis, C.J., Davies, J.A., Lockwood, M., Rouillard, A.P., Eyles, C.J., Harrison, R.A., 2009. Stereoscopic imaging of an earth-impacting solar coronal mass ejection: A major milestone for the STEREO mission. Geophysical Research Letters 36 (8) CiteID L08102.

Davies, J.A., Harrison, R.A., Rouillard, A.P., Sheeley, N.R., Perry, C.H., et al., 2009. A synoptic view of solar transient evolution in the inner heliosphere using the heliospheric imagers on STEREO. Geophysical Research Letters 36 (2) CiteID L02102.

Dasso, S., Nakwacki, M.S., Dmoulin, P., Mandrini, C.H., 2007. Progressive transformation of a flux rope to an ICME. Comparative analysis using the direct and fitted expansion methods. Solar Physics 244 (1–2), 115–137.

Démoulin, P., Dasso, S., 2009. Causes and consequences of magnetic cloud expansion. Astronomy and Astrophysics 498 (2), 551–566.

Eyles, C.J., Harrison, R.A., Davis, C.J., Waltham, N.R., Shaughnessy, B.M., Mapson-Menard, H.C.A., et al., 2009. The heliospheric imager onboard the STEREO spacecraft. Solar Physics 254 (2), 387–445.

Forsyth, R.J., Rees, A., Balogh, A., Smith, E.J., 2001. Magnetic field observations of transient events at ulysses, 1996–2000. Space Science Reviews 97, 217–220.

Galvin, A.B., Kistler, L.M., Popecki, M.A., Farrugia, C.J., Simunac, K.D.C., et al., 2008. The plasma and suprathermal ion composition (PLASTIC) investigation on the STEREO observatories. Space Science Reviews 136 (1–4), 437–486.

Gloeckler, G., Cain, J., Ipavich, F.M., Tums, E.O., Bedini, P., Fisk, L.A., et al., 1998. Investigation of the composition of solar and interplanetary matter using solar wind and pickup measurements with SWICS and SWIM on the ACE spacecraft. Space Science Reviews 86 (1–4), 492–539.

Gosling, J.T., Pizzo, V., Bame, S.J., 1973. Anomalously low proton temperatures in the solar wind following interplanetaryshock waves-evidence for magnetic bottles? Journal of Geophysical Research 78 2001–2009.

Gosling, J.T., McComas, D.J., 1987. Field line draping about fast coronal mass ejecta—a source of strong out-of-the-ecliptic interplanetary magnetic fields. Geophysical Research Letters 14, 355–358.

Gosling, J.T., Baker, D.N., Bame, S.J., Feldman, W.C., Zwickl, R.D., Smith, E.J., 1987. Bidirectional solar wind electron heat flux events. Journal of Geophysical Research 92, 8519–8535.

Gosling, J.T., Bame, S.J., McComas, D.J., Phillips, J.L., Scime, E.E., Pizzo, V.J., Goldstein, B.E., Balogh, A., 1994a. A forward-reverse shock pair in the solar wind driven by over-expanison of a coronal mass ejection: ULYSSES observations. Geophysical Research Letters 21 (3), 237–240.

Gosling, J.T., McComas, D.J., Phillips, J.L., Weiss, L.A., Pizzo, V.J., Goldstein, B.E., Forsyth, R.J., 1994b. A new class of forward-reverse shock pairs in the solar wind. Geophysical Research Letters 21 (12), 2271–2274.

Gulisano, A.M., Dmoulin, P., Dasso, S., Ruiz, M.E., Marsch, E., 2010. Global and local expansion of magnetic clouds in the inner heliosphere, Astronomy and Astrophysics (509), id.A39.

Harrison, R.A., Davis, C.J., Eyles, C.J., Bewsher, D., Crothers, S.R., et al., 2008. First imaging of coronal mass ejections in the heliosphere viewed from outside the Sun Earth line. Solar Physics 247 (1), 171–193.

Henke, T., Woch, J., Schwenn, R., Mall, U., Gloeckler, G., von Steiger, R., Forsyth, R.J., Balogh, A., 2001. Ionization state and magnetic topology of coronal mass ejections. Journal of Geophysical Research 106 (A6), 10597–10614.
Hirshberg, J., Bame, S.J., Robbins, D.E., 1972. Solar flares and solar wind helium enrichments: July 1965–July 1967. Solar Physics 23 (2), 467–486.
Howard, T.A., Three-dimensional reconstruction of coronal mass ejections using heliospheric imager data. Journal of Atmospheric and Solar-Terrestrial Physics, this issue, doi:10.1016/j.jastp.2010.08.009.
Howard, R.A., Sheeley Jr., N.R., Michels, D.J., Koomen, M.J., 1985. Coronal mass ejections—1979–1981. Journal of Geophysical Research 90 (September 1), 8173–8191.
Howard, R.A., Moses, J.D., Vourlidas, A., Newmark, J.S., Socker, D.G., Plunkett, S.P., Korendyke, C.M., et al., 2008. Sun Earth connection coronal and heliospheric investigation (SECCHI). Space Science Reviews 136 (1–4), 67–115.
Howard, T.A., Tappin, S.J., 2009. Interplanetary coronal mass ejections observed in the heliosphere: 1. Review of theory. Space Science Reviews 147 (1–2), 31–54.
Hudson, H.S., Bougeret, J.-L., Burkepile, J., 2006. Coronal mass ejections: overview of observations. Space Science Reviews 123, 13–30.
Illing, R.M.E., Hundhausen, A.J., 1986. Disruption of a coronal streamer by an eruptive prominence and coronal mass ejection. Journal of Geophysical Research 91 (October 1), 10951–10960.
Issautier, K., Perche, C., Hoang, S., Lacombe, C., Maksimovic, M., Bougeret, J.-L., Salem, C., 2005. Solar wind electron density and temperature over solar cycle 23: thermal noise measurements on wind. Advances in Space Research 35 (12), 2141–2146.
Jian, L., Russell, C.T., Luhmann, J.G., Skoug, R.M., 2006. Properties of interplanetary coronal mass ejections at one AU during 1995–2004. Solar Physics 239 (1–2), 393–436.
Kilpua, E.K.J., Luhmann, J.G., Gosling, J., Li, Y., Elliott, H., Russell, C.T., Jian, L., et al., 2009. Small solar wind transients and their connection to the large-scale coronal structure. Solar Physics 256 (1–2), 327–344.
Klein, L.W., Burlaga, L.F., 1982. Interplanetary magnetic clouds at 1 AU. Journal of Geophysical Research 87 (February 1), 613–624.
Lee, M., 2000. An analytical theory of the morphology, flows, and shock compressions at corotating interaction regions in the solar wind. Journal of Geophysical Research 105 (A5), 10491–10500.
Lepping, R.P., Wu, C.-C., Berdichevsky, D., Ferguson, T.J., 2008. Estimates of magnetic cloud expansion at 1 AU. Annales Geophysicae 26, 1919–1933.
Liu, Y., Davies, J.A., Luhmann, J.G., Vourlidas, A., Bale, S.D., Lin, R.P., 2010. Geometric triangulation of imaging observations to track coronal mass ejections continuously out to 1 AU. The Astrophysical Journal Letters 710 (1), L82–L87.
Low, B.C., 1994. Magnetohydrodynamic processes in the solar corona: flares, coronal mass ejections, and magnetic helicity. Physics of Plasmas 1 (5), 1684–1690.
Lugaz, N., Vourlidas, A., Roussev, I.I., Jacobs, C., Manchester IV, W.B., Cohen, O., 2008. The brightness of density structures at large solar elongation angles: what is being observed by STEREO SECCHI? The Astrophysical Journal 684 (2) 111–114.
Lugaz, N., Vourlidas, A., Roussev, I.I., Morgan, H., 2009. Solar-terrestrial simulation in the STEREO era: the 24–25 January 2007 eruptions. Solar Physics 256 (1–2), 269–284.
Luhmann, J.G., Curtis, D.W., Schroeder, P., McCauley, J., Lin, R.P., Larson, D.E., et al., 2008. STEREO IMPACT investigation goals, measurements, and data products overview. Space Science Reviews 136 (1–4), 117–184.
Manchester, W.B., Gombosi, T.I., Roussev, I., De Zeeuw, D.L., Sokolov, I.V., et al., 2004. Three-dimensional MHD simulation of a flux rope driven CME. Journal of Geophysical Research 109 (A1) (CiteID A01102).
McComas, D.J., Bame, S.J., Barker, P., Feldman, W.C., Phillips, J.L., Riley, P., Griffee, J.W., 1998. Solar wind electron proton alpha monitor (SWEPAM) for the advanced composition explorer. Space Science Reviews 86 (1/4), 563–612.
Mackay, D.H., Karpen, J.T., Ballester, J.L., Schmieder, B., Aulanier, G., 2010. Physics of solar prominences: II-magnetic structure and dynamics. Space Science Reviews 151 (4), 333–399.
Moon, Y.-J., Choe, G.S., Wang, H., Park, Y.D., Gopalswamy, N., Yang, G., Yashiro, S., 2002. A statistical study of two classes of coronal mass ejections. The Astrophysical Journal 581 (1), 694–702.
Möstl, C., Farrugia, C.J., Temmer, M., Miklenic, C., Veronig, A.M., Galvin, A.B., Leitner, M., Biernat, H.K., 2009. Linking remote imagery of a coronal mass ejection to its *in situ* signatures at 1 AU. The Astrophysical Journal Letters 705 (2), 180–185.
Newbury, J.A., Russell, C.T., Gedalin, M., 1998. The ramp widths of high-mach-number, quasi-perpendicular collisionless shocks. Journal of Geophysical Research 103 (A12), 29581–29594.
Owens, M.J., Merkin, V.G., Riley, P., 2006. A kinematically distorted flux rope model for magnetic clouds. Journal of Geophysical Research 111 (A3) CiteID A03104.
Palmer, I.D., Allum, F.R., Singer, S., 1978. Bidirectional anisotropies in solar cosmic ray events-evidence for magnetic bottles. Journal of Geophysical Research 83 (1), 75–90.
Pizzo, V.J., 1982. A three-dimensional model of corotating streams in the solar wind. III—magnetohydrodynamic streams. Journal of Geophysical Research 87 (June 1), 4374–4394.
Plunkett, S.P., Thompson, B.J., Howard, R.A., Michels, D.J., St. Cyr, O.C., Tappin, S.J., Schwenn, R., Lamy, P.L., 1997. LASCO observations of an Earth-directed coronal mass ejection on May 12. Geophysical Research Letters 25 (14), 2477–2480.
Pudovkin, M.I., Zaitseva, S.A., Benevolenska, E.E., 1979. The structure and parameters of flare streams. Journal of Geophysical Research 84, 6649–6652.
Richardson, I.G., Berdichevsky, D., Desch, M.D., Farrugia, C.J., 2000. Solar-cycle variation of low density solar wind during more than three solar cycles. Geophysical Research Letters 27 (23), 3761–3764.
Richardson, I.G., Cane, H.V., 2010. Interplanetary circumstances of quasi-perpendicular interplanetary shocks in 1996–2005. Journal of Geophysical Research 115 (A7) (CiteID A07103).
Riley, P., Lionello, R., Mikić, Z., Linker, J., 2008. Using global simulations to relate the three-part structure of coronal mass ejections to *in situ* signatures. The Astrophysical Journal 672 (2), 1221–1227.
Robbrecht, E., Patsourakos, S., Vourlidas, A., 2009. No trace left behind: STEREO observation of a coronal mass ejection without low coronal signatures. The Astrophysical Journal 701 (1), 283–291.
Rouillard, A.P., Davies, J.A., Forsyth, R.J., Rees, A., Davis, C.J., et al., 2008. First imaging of corotating interaction regions using the STEREO spacecraft. Geophysical Research Letters 35 (10), L10110.
Rouillard, A.P., Savani, N.P., Davies, J.A., Lavraud, B., Forsyth, R.J., et al., 2009a. A multispacecraft analysis of a small-scale transient entrained by solar wind streams. Solar Physics 256 (1–2), 307–326.
Rouillard, A.P., Davies, J.A., Forsyth, R.J., Savani, N.P., Sheeley, N.R., et al., 2009b. A solar storm observed from the sun to venus using the STEREO, venus express, and MESSENGER spacecraft. Journal of Geophysical Research 114 (A7) CiteID A07106.
Rouillard, A.P., Davies, J.A., Lavraud, B., Forsyth, R.J., Savani, N.P., Bewsher, D., et al., 2010a. Intermittent release of transients in the slow solar wind: I, remote sensing observations. Journal of Geophysical Research 115 (A4) CiteID A04103.
Rouillard, A.P., Lavraud, B., Davies, J.A., Savani, N.P., Burlaga, L.F., Forsyth, R.J., Sauvaud, J.-A., et al., 2010b. Intermittent release of transients in the slow solar wind: 2, *in situ* evidence. Journal of Geophysical Research 115 (A4) CiteID A0410.
Rouillard, A.P., Lavraud, B., Sheeley, N.R., Davies, J.A., Burlaga, L.F., Savani, N.P., Jacquey, C., Forsyth, R.J., 2010c. White light and *in situ* comparison of a forming merged interaction region. The Astrophysical Journal 719 (2), 1385–1392.
Russell, C.T., Shinde, A.A., 2003. ICME identification from solar wind ion measurements. Solar Physics 216 (1), 285–294.
Savani, N.P., Owens, M.J., Rouillard, A.P., Forsyth, R.J., Davies, J.A., 2010. Observational evidence of a coronal mass ejection distortion directly attributable to a structured solar wind. The Astrophysical Journal Letters 714 (1), L128–L132.
Sauvaud, J.-A., Larson, D., Aoustin, C., Curtis, D., Mdale, J.-L., Fedorov, A., et al., 2008. The IMPACT solar wind electron analyzer (SWEA). Space Science Reviews 136 (1–4), 227–239.
Sheeley Jr., N.R., Howard, R.A., Michels, D.J., Koomen, M.J., Schwenn, R., et al., 1985. Coronal mass ejections and interplanetary shocks. Journal of Geophysical Research 90 (January 1), 163–175.
Sheeley Jr., N.R., Wang, Y.-M., Hawley, S.H., Brueckner, G.E., Dere, K.P., Howard, R.A., Koomen, M.J., Korendyke, et al., 1997. Measurements of flow speeds in the corona between 2 and 30 R sub sun. Astrophysical Journal 484, 472.
Sheeley, N.R., Walters, J.H., Wang, Y.M., Howard, R.A., 1999. Continuous tracking of coronal out flows: two kinds of coronal mass ejections. Journal of Geophysical Research 104, 24739–24768.
Sheeley Jr., N.R., Herbst, A.D., Palatchi, C.A., Wang, Y.-M., et al., 2008a. SECCHI observations of the Sun's garden-hose density spiral. The Astrophysical Journal 674 (2), L109–L112.
Sheeley Jr., N.R., Herbst, A.D., Palatchi, C.A., Wang, Y.-M., et al., 2008b. Heliospheric images of the solar wind at Earth. The Astrophysical Journal 675 (1), 853–862.
Sheeley, N.R., Lee, D.D.-H., Casto, K.P., Wang, Y.-M., Rich, N.B., 2009. The structure of streamer blobs. The Astrophysical Journal 694 (2), 1471–1480.
Sheeley, N.R., Rouillard, A.P., 2010. Tracking streamer blobs into the heliosphere. The Astrophysical Journal 715 (1), 300–309.
Smith, C.W., L'Heureux, J., Ness, N.F., Acua, M.H., Burlaga, L.F., Scheifele, J., 1998. The ACE magnetic fields experiment. Space Science Reviews 86 (1/4), 613–632.
Schmidt, J.M., Cargill, P.J., 2003. Magnetic reconnection between a magnetic cloud and the solar wind magnetic field. Journal of Geophysical Research 108 (A1), SSH5-1. doi:10.1029/2002JA009325.
Schwenn, R., Rosenbauer, H., Muehlhaeuser, K.-H., 1980. Singly-ionized helium in the driver gas of an interplanetary shock wave. Geophysical Research Letters 7, 201–204.
Tappin, S.J., Howard, T.A., 2009. Direct observation of a corotating interaction region by three spacecraft. The Astrophysical Journal 702 (2), 862–870.
Thernisien, A., Vourlidas, A., this issue. Journal of Atmospheric and Solar-Terrestrial Physics, submitted.
Thernisien, A., Vourlidas, A., Howard, R.A., 2009. Forward modeling of coronal mass ejections using STEREO/SECCHI data. Solar Physics 256 (1–2), 111–130.
Vourlidas, A., Howard, R.A., 2006. The proper treatment of coronal mass ejection brightness: a new methodology and implications for observations. The Astrophysical Journal 642 (2), 1216–1221.
Wang, Y.-M., Sheeley Jr., N.R., Howard, R.A., Kraemer, J.R., Rich, N.B., Andrews, M.D., Brueckner, G.E., et al., 1997. Origin and evolution of coronal streamer structure during the 1996 minimum activity phase. Astrophysical Journal 485, 875.
Wang, Y.-M., Sheeley Jr., N.R., Walters, J.H., Brueckner, G.E., Howard, R.A., et al., 1998. Origin of streamer material in the outer corona. Astrophysical Journal Letters 498, 165.
Wang, Y.-M., Sheeley Jr., N.R., Rouillard, A.P., 2006. Role of the Sun's nonaxisymmetric open flux in cosmic-ray modulation. The Astrophysical Journal 644 (1), 638–645.

Webb, D.F., Howard, R.A., 1994. The solar cycle variation of coronal mass ejections and the solar wind mass flux. Journal of Geophysical Research 99 (A3), 4201–4220.

Webb, D.F., Lepping, R.P., Burlaga, L.F., DeForest, C.E., Larson, D.E., Martin, S.F., Plunkett, S.P., Rust, D.M., 2000. The origin and development of the May 1997 magnetic cloud. Journal of Geophysical Research 105 (A12), 27251–27260.

Wood, B.E., Howard, R.A., Thernisien, A., Socker, D.G., 2009. An empirical reconstruction of the 2008 April 26 coronal mass ejection. The Astrophysical Journal 702 (2), 901–910.

Wood, B.E., Howard, R.A., Socker, D.G., 2010a. Reconstructing the morphology of an evolving coronal mass ejection. The Astrophysical Journal 715 (2), 1524–1532.

Wood, B.E., Howard, R.A., Thernisien, A., Socker, D.G., 2010b. The three-dimensional morphology of a corotating interaction region in the inner heliosphere. The Astrophysical Journal Letters 708 (2), 89–94.

Xiong, M., Zheng, H., Wu, S.T., Wang, Y., Wang, S., 2007. Magnetohydrodynamic simulation of the interaction between two interplanetary magnetic clouds and its consequent geoeffectiveness. Journal of Geophysical Research 112 (A11) CiteID A11103.

Xiong, M., Zheng, H., Wang, S., 2009. Magnetohydrodynamic simulation of the interaction between two interplanetary magnetic clouds and its consequent geoeffectiveness: 2. Oblique collision. Journal of Geophysical Research 114 (A11) CiteID A11101.

Yurchyshyn, V., Yashiro, S., Abramenko, V., Wang, H., Gopalswamy, N., 2005. Statistical distributions of speeds of coronal mass ejections. The Astrophysical Journal 619 (1), 599–603.

Zhang, J., Dere, K.P., Howard, R.A., Vourlidas, A., 2004. A study of the kinematic evolution of coronal mass ejections. The Astrophysical Journal 604 (1), 420–432.

Zurbuchen, T.H., Fisk, L.A., Lepri, S.T., von Steiger, R., 2003. The composition of interplanetary coronal mass ejections. In: SOLAR WIND TEN: Proceedings of the 10th International Solar Wind Conference, vol. 679, pp. 604–607.

Zurbuchen, T.H., Richardson, I.G., 2006. *In situ* solar wind and magnetic field signatures of interplanetary coronal mass ejections. Space Science Reviews 123 (1–3), 31–43.